Desalination and Water Treatment
www.deswater.com

doi: 10.5004/dwt.2017.20140

63 (2017) 193–202
February

Plant extract-stabilized nanoiron for the treatment of aqueous paraquat in the presence of H_2O_2 and UV light

Pannipa Sukthang, Patcharaporn Phuinthiang, Manee Jindakaraked, Jirapat Ananpattarachai*, Puangrat Kajitvichyanukul*

Center of Excellence on Environmental Research and Innovation, Faculty of Engineering, Naresuan University, Phitsanulok, Thailand 65000, emails: jirapata@nu.ac.th (J. Ananpattarachai), puangratk@nu.ac.th (P. Kajitvichyanukul), jaopannie@gmail.com (P. Sukthang), ryeoploy@gmail.com (P. Phuinthiang), ramfin_jin@hotmail.com (M. Jindakaraked)

Received 20 April 2016; Accepted 31 July 2016

ABSTRACT

This work aimed to increase the working ability of iron nanoparticles in Fenton and photo-Fenton process by preventing the aggregation of the catalysts using the plant extract with a green chemistry approach. We used extracts from tea, coffee, and garlic as stabilizing agents to cap the iron nanoparticles. Various iron nanoparticles were used to remove paraquat, a known herbicide presented in agricultural wastewater, from aqueous solution. The organic molecules from the plant extract induced the decreasing of the pH_{pzc} toward a very low acidic pH. The values of pH_{pzc} of iron nanoparticles were lower from 4.1 (without plant extract) to 1.6 with tea extract resulting in the high adsorption ability of paraquat. Among three types of catalysts, the iron nanoparticles obtained from tea extract provided the highest degradation percentage of paraquat using Fenton and photo-Fenton processes. It was found that the maximum removal percentage of paraquat was obtained within 20 min. The kinetic data of all types of iron nanoparticles was well explained by pseudo-first-order pattern with the reaction constants in the range of 1.83–3.82 × 10^{-2} min^{-1} for Fenton process and 7.27–10.94 × 10^{-2} min^{-1} for photo-Fenton process.

Keywords: Fenton; Nanoparticles; Paraquat; Green chemistry; Chemical oxidation; Nanomaterial

1. Introduction

Nanoscale iron particles are recently gaining considerable interest in environmental protection and remediation. These iron nanoparticles contain iron oxides in the form of magnetite or maghemite. They can be used as a Fenton-like catalyst for the degradation of aqueous organic solutes [1,2]. They have been found to be effective in degrading various chlorinated organic contaminant hydrocarbons in the wastewater stream [3–5]. However, the drawback of these particles was known as they tend to agglomerate rapidly to form larger aggregates due to Van der Waals and magnetic forces resulting in less efficiency in pollutant removal [6].

Both physical and chemical methods have been used to synthesize the iron nanoparticles. The physical methods included thermal decomposition, vacuum sputtering, and milling consume a large amount of energy [7,8]. The well-known chemical process is the synthesizing of iron nanoparticles using sodium borohydride ($NaBH_4$), a toxic reducing agent. It is known that this reducing chemical is potentially harmful to the environment and may additionally involve a volatile organic solvent such as toluene or chloroform [8]. The corrosiveness and flammability of this chemical are also reported [9].

In this work, we proposed the green synthesis by applying the stabilizer from plant extracts that are the environmental friendly agents to substitute the classical method using the toxic $NaBH_4$. The green synthesis is a part of green chemistry which the utilization of a set of principles reduces or

* Corresponding author.

eliminates the use or generation of hazardous substances in the design, manufacture, and application of chemical products [6]. The choice of an environmentally compatible solvent system, an eco-friendly reducing agent, and a non-hazardous capping agent for stabilizing the nanoparticles are three main criteria for a "green" nanoparticle synthesis. Besides being the benign environmental process, this green synthesis can also improve the stability of iron nanoparticles from the agglomeration by capping technique. It is known that the aggregation of the iron nanomaterial leads to the reducing of surface area to volume ratio. However, less work demonstrated the performance of these green nanoparticles especially the iron nanoparticles in the application of water and wastewater treatment in comparison with the nanoparticles obtained from the classical method.

To explore the ability of iron nanoparticles obtained from green synthesis, paraquat, the most widely used herbicide was chosen as the pollutant in concerned. Paraquat or 1,1′-dimethyl-4,4′-bipyridinium chloride is considered as a potent human poison as a possible carcinogen [10]. World Health Organization has recommended the maximum concentration of paraquat in drinking water at, 40 μg/L [10]. The development of efficient procedures for the removal of paraquat from contaminated wastewater are continuously increased due to its continuous use and high toxicity [11–13].

The major purpose of this work was to investigate the ability of green iron nanoparticles in degradation of organic pollutants using Fenton and photo-Fenton processes. Our extracted plants to be used as a capping agent for the investigated iron nanoparticles were tea, coffee, and garlic. The extracts contained molecules bearing alcohol functional group [6]. These extracts were used as stabilizers to obtain various iron nanoparticles from a hydrothermal method. Transmission electron microscopy (TEM), Fourier transform-infrared spectroscopy (FTIR) and X-ray diffraction analyzer (XRD) were performed to ascertain the characteristics of iron nanoparticles. The experiments and kinetics in degradation of paraquat using heterogeneous Fenton and photo-Fenton processes by the four types of iron nanoparticles were conducted. The performance in term of paraquat removal efficiency and mineralization ability (as measured by total organic carbon (TOC) parameters) are discussed. In this work, the green capping agents have demonstrated the prevention of the aggregation behavior of the iron nanoparticles and, consequently, the performance of the Fenton and photo-Fenton processes in paraquat removal was tremendously enhanced by these green iron nanoparticles.

2. Methodology

2.1. Materials

All the materials used in this study were of analytical grade and required no further purification. Heptahydrate ferrous sulfate ($FeSO_4 \cdot 7H_2O$), ferric chloride ($FeCl_3$), Hydrogen peroxide solution (H_2O_2, 35%, w/w) and sodium hydroxide (NaOH) were purchased from Aldrich. Aqueous acetic acid solution 99.8% was from Merck (Germany).

Garlic, coffee, and green tea were purchased from a local grocery store (Phitsanulok, Thailand). Garlic was peeled and then rinsed with deionized water before use. Coffee and green tea leaves were chopped and rinsed in the same manner with garlic. All glasswares were washed and rinsed with deionized water, followed by subsequent drying. All the aqueous solutions were prepared using distilled deionized water (18.2 M Ω cm^{-1}).

2.2. Synthesis of iron nanoparticles from co-precipitation method

For iron nanoparticles from co-precipitation method, Fe(II) and Fe(III) salts ($FeSO_4$ and $FeCl_3$, Aldrich) with molar ratio 1:2 were dissolved in 400 mL deionized water (deaerated with Ar) under vigorous stirring in the inert atmosphere. Then, 15 mL of NH_4OH was quickly added to the solution and black precipitates of magnetite were obtained. To activate iron nanoparticles, 1.5 M $NaBH_4$ was added to the batch reactor containing 3 g/L of the magnetite in deionized water. After 24 h of shaking, the iron nanoparticles were removed and washed three times with deionized water.

2.3. Synthesis of iron nanoparticles from green chemistry method

For iron nanoparticles from green chemistry method, the Fe(II) and Fe(III) salts with molar ratio 1:2 were dissolved in 400 mL deionized water. The precipitated magnetite particles were obtained by the addition of 15 mL of NH_4OH to the solution. They were collected for the further mixing with the plant extracts.

For coffee extract, approximately 20 g of coffee (or green tea) dry leave was chopped, added to 1 L of deionized water, and allowed to sit at room temperature for 24 h. The resulting extract solution was decanted, and the solid coffee pieces were removed. To prepare the iron nanoparticles, the 0.24 g of precipitated magnetite particles was mixed with 5 ml of coffee (or green tea) extract and shaken to ensure thorough mixing. The mixture was put into the microwave and heated at 60°C for 1 min. The chemicals were dried at 100°C for 90 min and put in a vacuum chamber.

For garlic extract, approximately 7 g of garlic was chopped (not crushed) into small pieces, added to 50 mL of deionized water, and left at room temperature for 24 h. The resulting extract solution was decanted to collect a pale white transparent solution, and the solid garlic pieces were removed. For iron nanoparticles using garlic extract, 5 mL of acetic acid (with 99.8% concentration in a volume of 100 mL deionized water) was added to the 5 ml of garlic extract. Then, 0.24 g of magnetite particles was added to the solution, and all steps were repeated in the same manner with iron nanoparticles from the coffee extract.

The iron nanoparticles were then separated first by evaporating water from the iron solution on a hot plate, and then by drying it overnight in a fume hood.

2.4. Material characterization

The surface physical morphology of iron nanoparticles was examined using a scanning electron microscope (SEM) (Leo1455VP). In the SEM analysis, the samples were coated with a thin layer of gold and mounted on a copper stab using a double stick carbon tape. For TEM (Philips/Tecnai 12), the samples were dispersed in 5 mL water. TEM grids were prepared by placing a drop of the particle dispersion

on a carbon-coated copper grid and drying at room temperature. All samples were analyzed by an X-ray diffractometers (PANalytical/X'pert) using Cu Kα radiation in the range of 20°–70°.

FTIR were recorded at room temperature on a Perkin Elmer Spectrum BX spectrophotometer. The infrared spectra were recorded in the 4,000–400 cm^{-1} range using KBr pellets for determination of the presence of organic molecules on the iron nanoparticles. The surface area of iron nanoparticles was measured by the surface area analyzer (Quantachrome Instruments NOVA 2200e). Each sample was out-gassed at 110°C for 24 h before being placed in a 77 K liquid nitrogen bath with nitrogen gas adsorbate. The surface area of each sample was calculated by the Brunauer–Emmett–Teller (BET) equation. The pore size distributions over the mesopore region were calculated using the Barrett–Joyner–Halenda (BJH) equation.

The values of point of zero charge (PH_{pzc}) of the iron nanoparticles were determined by phase analysis light scattering employing a ZetaSizer (Nano ZS90, Malvern, UK). The measurement angle was 90° to the incident light. Data were collected for 10 cycles. The zeta potential was calculated from the electrophoretic mobility using the Smoluchowski approximation approach [14].

2.5. Fenton and photo-Fenton experiments

All UV/H_2O_2, Fenton and photo-Fenton experiments were performed in a batch reactor. The cylindrical reactor with 1.1 L volume and was made from quartz glass (ACE Glass Co. 7841-06; Vineland, NJ). In UV/H_2O_2 and photo-Fenton experiments, a 10 W germicide lamp with a principal wavelength of 254 nm was used as the light source. The intensity of the incident light inside the photoreactor was measured as 0.50×10^{-6} Einstein s^{-1} by uranyl actinometer method. The germicide lamp was inserted into a double-walled quartz immersion well, located at the center of the reactor. The fresh tap water was flushed through the immersion well to prevent the lamp from overheating. The solution was fully stirred with a magnetic stirrer to ensure sufficient mixing. The reaction temperature was kept constant at 25°C. The reaction period for all experiments in this work is 90 min unless otherwise specified. The experimental setup is shown in schematic diagram (Fig. 1).

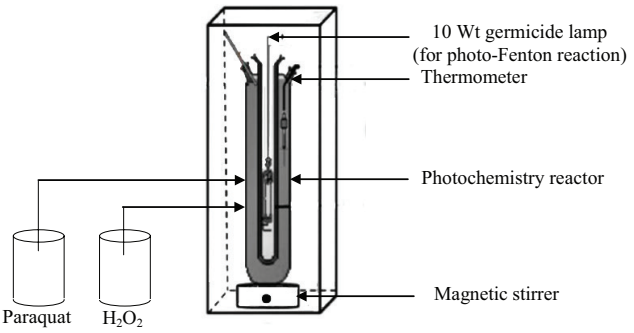

Fig. 1. Schematic diagram of the Fenton and photo-Fenton reactions to remove paraquat from aqueous solution using green iron nanoparticles.

In Fenton process, the initial concentration of paraquat was 60 mg/L with an initial TOC value of 32 mg/L in aqueous solution. The pH value of the solution was set at 3 by the addition of a H_2SO_4 solution before startup. For heterogeneous Fenton process, 0.3 g of iron nanoparticles was added and thoroughly mixed with the paraquat-contaminated water before the addition of a given volume of hydrogen peroxide.

For the photo-Fenton process, the initial concentration of paraquat was 200 mg/L with an initial TOC value of 98 mg/L. The time at which the 10 Wt germicide lamp was turned on was considered as time zero or the beginning of the experiment that was taking place simultaneously with the addition of hydrogen peroxide. Fenton and photo-Fenton reactions cannot occur at pH > 10. Therefore, the reaction was stopped instantly by adding NaOH to the reaction mixtures and quenched by adding Na_2SO_3 to remove H_2O_2 before analysis. During the experiments, samples were withdrawn from the reactor at time intervals for analysis.

After complete Fenton and photo-Fenton processes, iron nanoparticles were magnetically separated from the solution and washed three times with deionized water for the comparison experiments between fresh and recycled iron nanoparticles. Paraquat concentration was detected by a colorimetric method using UV-Vis spectrophotometer by reducing paraquat to the blue radical. A solution sample in the test tube was added with 0.1% sodium dithionite in 0.1 M sodium hydroxide. The mixture was gently mixed and measured for light absorbance within 1 min. The detection was done at 600 nm wavelength using the spectrophotometer. The samples were filtrated through GF/C to remove any particulate matter before using spectrophotometer determination. Initial and treated TOC were analyzed with a Shimadzu 700 TOC ANALYZER 0-1 Analytical after filtration. Hydrogen peroxide was measured by the standard iodometric titration method. Experiments were done in triplicate for the same set of conditions. The variations were systematically within ±10% of the stated values.

3. Results and discussion

3.1. Characterization of iron nanoparticles

Crystal sizes of iron nanoparticles were obtained from TEM analysis and shown in Fig. 2. The iron nanoparticles obtained from coffee, tea, and garlic extracts were Fe/C, Fe/T, and Fe/G, respectively. The characteristics of iron nanoparticles from co-precipitation using $NaBH_4$ (as Fe) were also analyzed for comparison purpose. From TEM results, the iron nanoparticles have a semispherical shape with the size in the range of 20–60 nm. The iron nanoparticles of varying sizes were formed using different types of plant extract. Crystal size and surface area of three types of iron nanoparticles were shown in Table 1. Apparently, the crystal sizes of Fe/C, Fe/G, and Fe/T are bigger than those of Fe from co-precipitation process.

Chemical analysis of the iron nanoparticles by FTIR was used to determine the existence of stabilizing plant extract as shown in Fig. 3. Results from spectra of all types of iron nanoparticles exhibited the clear peaks representing the presence of organic molecules from plant extract in the composition of iron nanoparticles. Results from TEM and FTIR

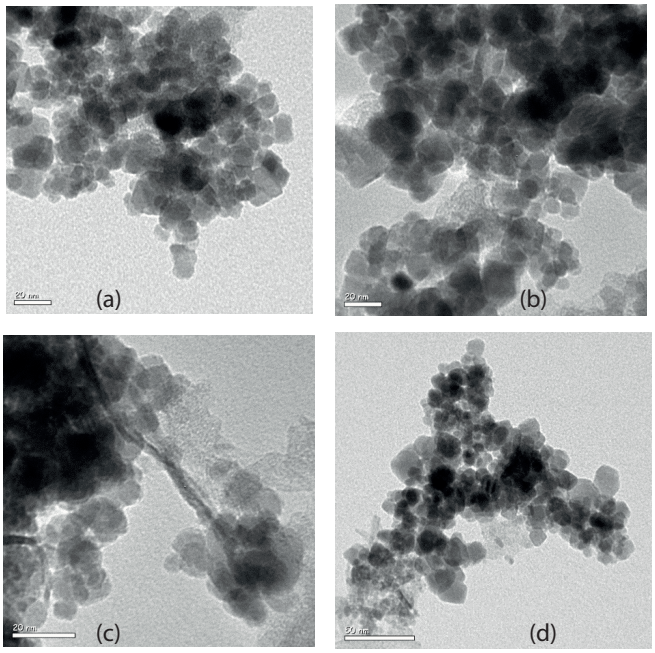

Fig. 2. TEM images of iron nanoparticles (a) Fe, (b) Fe/G, (c) Fe/T, and (d) Fe/C.

Table 1
Crystal size, and size distribution of various types of iron nanoparticles

Type	Crystal size (nm)	Surface area (m^2/g)
Fe	30.1 ± 12.5	21.85
Fe/G	36.05 ± 13.7	16.701
Fe/C	42.5 ± 15.4	14.586
Fe/T	39.6 ± 17.3	15.701

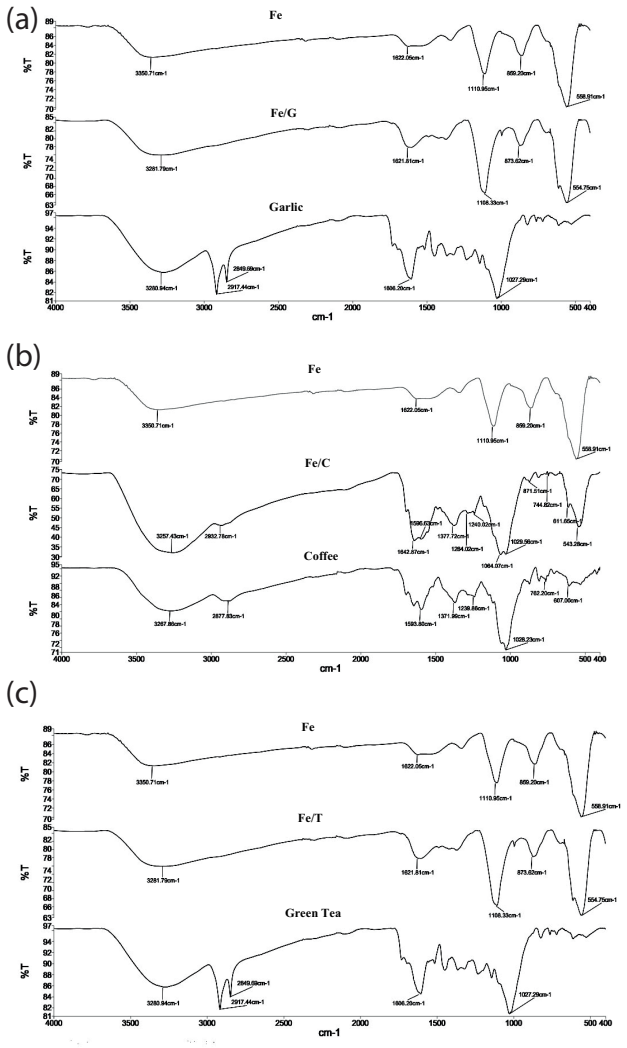

Fig. 3. Comparison of, FTIR spectra of iron nanoparticles without plant extract (Fe), iron nanoparticles with plant extract (Fe/G, Fe/C, or Fe/T), and plant extracts (Garlic, Coffee, or Green Tea) for (a) Fe/G, (b) Fe/C, and (c) Fe/T.

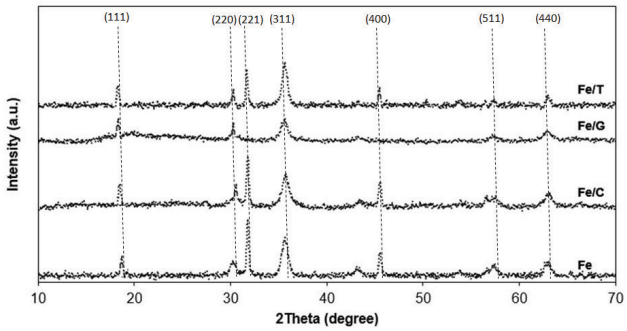

Fig. 4. XRD patterns of Fe, Fe/C, Fe/G and Fe/T.

are the evidence showing that the organic molecules from extracts tended to cap the iron nanoparticles. Moreover, these capping agents stabilized iron nanoparticles and prevented them from the agglomeration. The aggregation might have occurred in the absence of any coating agent or organic moieties on the surface of the particles. These organic chemicals from tea and coffee extracts are polyphenols and caffeine while the organic molecules from garlic are mainly organosulfur compounds such as diallyl sulfides and alicin [15]. From our works, the iron nanoparticles from tea and coffee extracts dispersed better than those from garlic extracts.

The XRD patterns of Fe, Fe/C, Fe/G, and Fe/T are shown in Fig. 4. From many previous works, the magnetite has the diffraction peaks indicated 111, 220, 311, 400, 511, 440 [16,17] and the maghemite has the different peaks indicated 210, 211, 220, 311, 400, 620 [18]. Also, the maghemite phase is known to exhibit few extra peaks at 23.77° (210) and 26.10° (211) which can be used to distinguish the maghemite from the magnetite phase. The small peak at 18.20° (111) can be used to identify the magnetite phase. Therefore, the obtained XRD spectrum corresponds to the pattern that is expected for a crystalline magnetite (Fe_3O_4) phase. The XRD patterns of Fe/C and Fe/T were similar because both extracts contained caffeine and polyphenols chemicals which can form complexes with metal ions in solution and reduce them to the corresponding metals [17]. The supplementary data shows the consistency of the characteristics of iron nanoparticles such as sizes and phases.

3.2. Paraquat removal by iron nanoparticles without H_2O_2 addition

Prior to the additions of H_2O_2 in Fenton process, the iron nanoparticles were equilibrated with paraquat solution. Residual fractions of paraquat in aqueous solution after 50 min were measured as shown in Fig. 5(a). The adsorbed paraquat concentrations on the surface of iron nanoparticles were also calculated from the subtraction of the residual paraquat from the initial concentration of paraquat. Also, the concentrations of paraquat extracted by solid extraction method from the iron nanoparticles were also analyzed. It was found that the value of adsorbed paraquat from solid extraction method and calculation method are in the same range for each type of iron nanoparticles. The different amounts of paraquat adsorbed on the surface of various types of iron nanoparticles at pH 3 and obtained from the calculation method are depicted in Fig. 5(b).

Results show that equilibrium time of paraquat in aqueous solution after treatment with all four types of iron nanoparticles was not significantly different. Within the concentration range studied; the sorption process of paraquat on iron nanoparticles closely approached equilibrium within 30 min. No significant changes were observed after 1 h. The amounts of paraquat adsorbed per unit weight of iron nanoparticles (or x/m) were 33.83, 27.10, 19.58, and 9.65 mg/g for Fe/T, Fe/C, Fe/G and Fe, respectively.The surface adsorption differences are commonly explained by the BET specific surface area. However, in our work, the specific surface areas of four types of iron nanoparticles were slightly different. Although, the BET specific surface area of Fe nanoparticles was 21.85 m^2/g which higher than that of other green nanoparticles, the sorbed proportions of paraquat onto Fe nanoparticles are considerably lowest.

In considering the electrostatic interaction between paraquat and iron nanoparticles, the values of point of zero charge (pzc) for all four iron nanoparticles were determined as shown in Fig. 6 and Table 2. The pH_{pzc} of Fe/T, Fe/C, Fe/G and Fe were found at 1.6, 2.2, 3.3, and 4.1, respectively. Thus, the surface of iron nanoparticles is positively charged when pH is lower than pH_{pzc} and negatively charged when pH is greater than pH_{pzc}. It is known that the pK_a of cationic paraquat was about 9–9.5 [15]. Thus, cationic paraquat is readily adsorbed on a negatively-charged surface. It is cleared that at pH 3 the Fe/T, and Fe/C are negatively-charged surfaces while the Fe/G and Fe are the positively-charged surface. The high adsorption of paraquat would occur on the surface of Fe/T and Fe/C, and the minimal adsorption of paraquat on the surface of Fe/G and Fe would be expected. Our results showed that

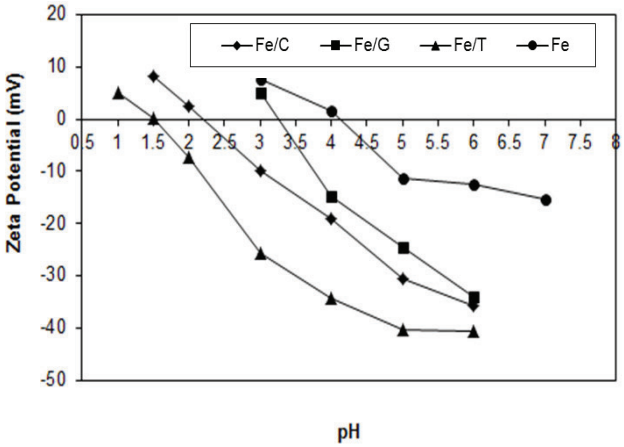

Fig. 6. Zeta potential of various iron nanoparticles as a function level of pH.

Table 2
pH_{pzc} of various types of iron nanoparticles

Iron nanoparticles	Source of extract	Organic chemicals in plant extract	pH_{pzc}
Fe/T	Tea	Polyphenol and caffeine	1.6
Fe/C	Coffee	Polyphenol and caffeine	2.2
Fe/G	Garlic	Organosulfur (diallyl sulfides and alicin)	3.3
Fe	–	–	4.1

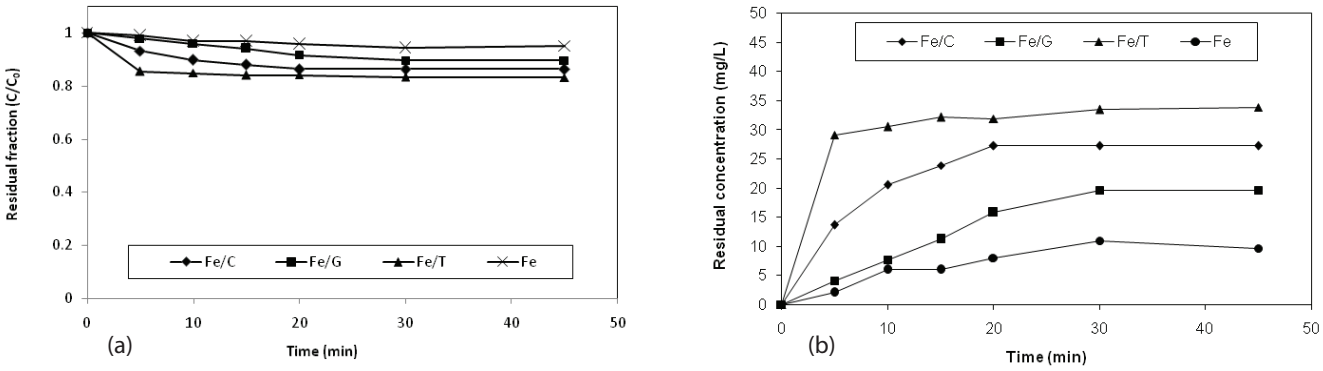

Fig. 5. Comparison of (a) residual fraction of paraquat in aqueous solution in the presence of iron nanoparticles (without H_2O_2) and (b) adsorbed mass of paraquat onto surface of various types of iron nanoparticles. Conditions: C_0= 60 mg/L, dose of iron nanoparticles = 0.3 g/L, and pH 3.

the Fe iron nanoparticles provided the lowest adsorption of paraquat while the Fe/T provided the highest adsorption. Hence, the capping of organic chemicals from extracts effectively shifted the pH_{pzc} toward a very low pH. The surface charge of green iron nanoparticles from polyphenol and caffeine agents becomes negative upon increase of pH beyond the pH_{pzc} and vice-versa.

Thus, in the presence of iron nanoparticles and absence of H_2O_2, the paraquat can be removed from the aqueous solution. The adsorption via electrostatic attraction between paraquat and iron nanoparticles tends to be the major mechanism for this removal. As the by-product of paraquat derivatives are not detectable by GC/MS measurement, the transformation of paraquat by chemical degradation does not occur during this experiment.

3.3. Paraquat removal by Fenton processes using green iron nanoparticles

Fig. 7(a) illustrates the degradation of paraquat with the initial concentration of 60 mg/L by green iron nanoparticles and Fe from co-precipitation to compare their degradation abilities. The removal efficiencies of paraquat by Fe/T, Fe/C, Fe/G, and Fe in Fenton process were 57.78%, 52.2%, 40%, and 36% after 90 min reaction, respectively. The residual concentration of H_2O_2 during Fenton reaction is shown in Fig. 7(b). The paraquat removal by adsorption and Fenton reaction using various types of green iron nanoparticles is also shown in Fig. 7(c).

This result indicates that the green nanoparticles from plant extracts can provide higher efficiency that those from co-precipitation method. As the stabilizing agent, the plant extracts can prevent the particle agglomeration which possibly causes the well-dispersion of nanoparticles in the solution and increases the efficiency of Fenton reaction in pollutant degradation.

Following the suggestions of several authors [18,19], Fenton and photo-Fenton reactions are well represented by using pseudo-first-order kinetics for the initial times. The kinetic constant (k) was determined by the following expression:

$$\ln\left(\frac{C_t}{C_0}\right) = kt$$

where C_0 represents, the initial concentration of the organic compound and C represents the concentration of the organic compound as a function of time, t.

The reaction rates and kinetic constants of paraquat degradation using different types of iron nanoparticles were also calculated as shown in Table 3.

Results show that within 90 min of Fenton process, the degradation rate of paraquat was 2.6266, 1.8127, 1.1632 and 1.0353 mg/L-min for Fe/T, Fe/C, Fe/G and Fe, respectively. This pattern suggests that the reaction rate can be enhanced by the capping of the organic molecule on the surface of iron nanoparticles. The reaction rate enhancement of the Fe/T was double higher than that of the Fe from co-precipitation method. The rate constant of the Fenton process using Fe was only 1.83×10^{-2} min^{-1}, whereas the rate constant of the Fe/T was 3.82×10^{-2} min^{-1}. This increase may have been attributed to the well-dispersion of iron nanoparticles as discussed previously.

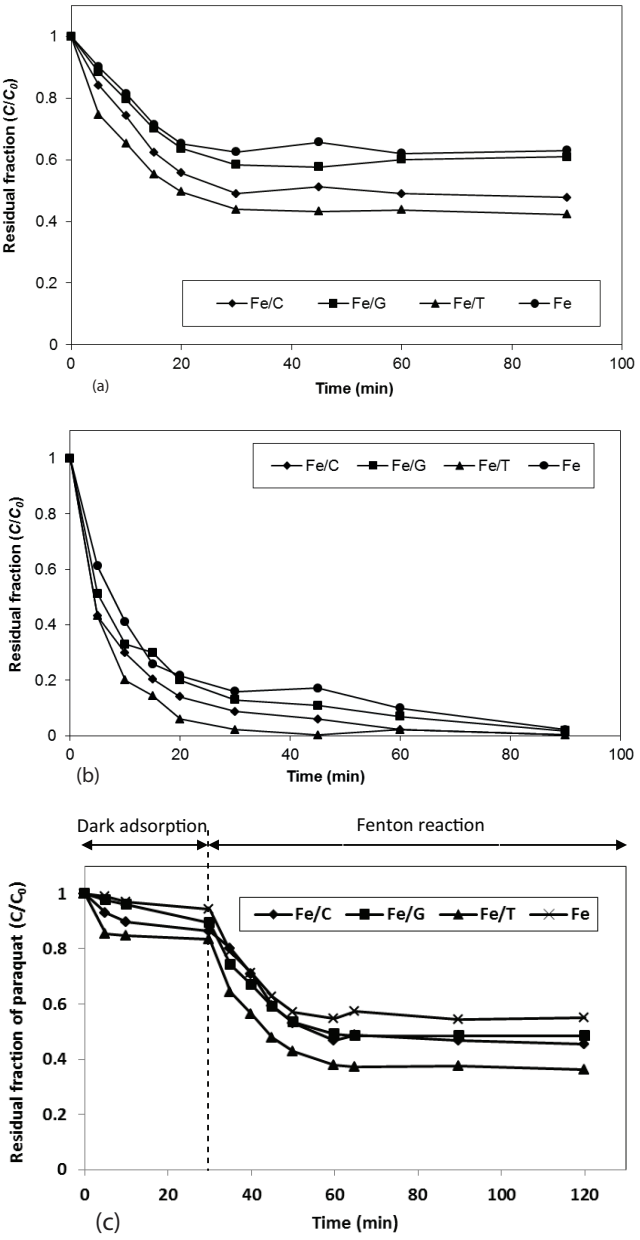

Fig. 7. Comparison of (a) paraquat degradation by Fenton reaction, (b) residual concentration of H_2O_2 and (c) paraquat removal by adsorption and Fenton reaction using various types of green iron nanoparticles. Conditions: C_0= 60 mg/L, dose of iron nanoparticles = 0.3 g/L, Fe:H_2O_2 = 1:0.8 molar ratio, and pH 3.

3.4. Paraquat removal by photo-Fenton processes using green iron nanoparticles

This experiment set was conducted using 200 mg/L initial concentration of paraquat and 98 mg/L of TOC in aqueous solution. Before the photo-Fenton experiment, the reaction

Table 3
Values of kinetic parameters including initial rate, r, kinetic constant, k and half-life of paraquat, $t_{1/2}$, based on the Fenton process of various types of iron nanoparticles

Iron Nanoparticles	Kinetic parameters				% Removal efficiency after 120 min	Rate increase
	r (mg/L-min)	$k_{obs} \times 10^{-2}$ (min^{-1})	R^2	$t_{1/2}$ (min)		
Fe	1.0353	1.83	0.9168	37.88	37.98	–
Fe/G	1.1632	2.02	0.9473	34.31	39.90	1
Fe/C	1.8127	2.67	0.9499	25.96	51.04	1
Fe/T	2.6266	3.82	0.9451	18.15	56.28	2

between paraquat and H_2O_2 was performed. When paraquat was in contact with H_2O_2 under illumination, the removal percentage of paraquat was equal to 43%. Indeed, H_2O_2 undergoes direct photolysis when the light wavelength, λ, is <360 nm [20] and produces HO$^{\bullet}$ radical according to equation below:

$$H_2O_2 + h\nu \rightarrow 2HO^{\bullet} \quad (1)$$

The UV lamp in our work emitted light at a wavelength 245 nm. So the paraquat in our work was partially degraded without the catalyst. Also, the disappearance of paraquat due to the evaporation was less than 5% for 90 min experimental period. This result indicated that the potential loss of paraquat by volatilization was not significant during the degradation of paraquat in the Fenton and photo-Fenton process.

The UV irradiation was introduced to let the photo-Fenton occurred to enhance the degradation of paraquat using iron nanoparticles. The removal of paraquat by photo-Fenton using different types of green iron nanoparticles and Fe from co-precipitation is shown in Fig. 8(a). The residual concentration of H_2O_2 in the photo-Fenton reaction is shown in Fig. 8(b). The performance of paraquat removal by adsorption (without H_2O_2 and UV light) and photo-Fenton reaction using various types of green iron nanoparticles is also shown in Fig. 8(c).

The degradation ability of all iron nanoparticles in the photo-Fenton process can be ranked in the following order: Fe/T > Fe/C > Fe/G > Fe, which is similar to that in Fenton process. However, it is worth to emphasize that the degree of paraquat removal of all green iron nanoparticles using photo-Fenton was not significantly different. The UV irradiation accelerated the reaction and the abundant amounts of HO$^{\bullet}$ were occurred in a short time and led to a series of reaction that can degrade paraquat effectively with regardless of types of green iron nanoparticles.

The values of kinetic parameters including initial rate, r, kinetic constant, k and half-life of paraquat, $t_{1/2}$, based on the photo-Fenton process also are shown in Table 4. The degradation efficiency of paraquat using Fe/T, Fe/C, Fe/G and Fe was 88.0%, 84.6%, 80.7%, and 80.0%, respectively. The pseudo first-order kinetic rate of paraquat degradation using Fe/T (min^{-1}) was slightly higher than that using Fe (min^{-1}). A rapid degradation of paraquat occurred in the first 5 min and then reached equilibrium within 10 min. These results also suggest that the heterogeneous photo-Fenton oxidation of paraquat based on iron nanoparticles worked better than the Fenton process.

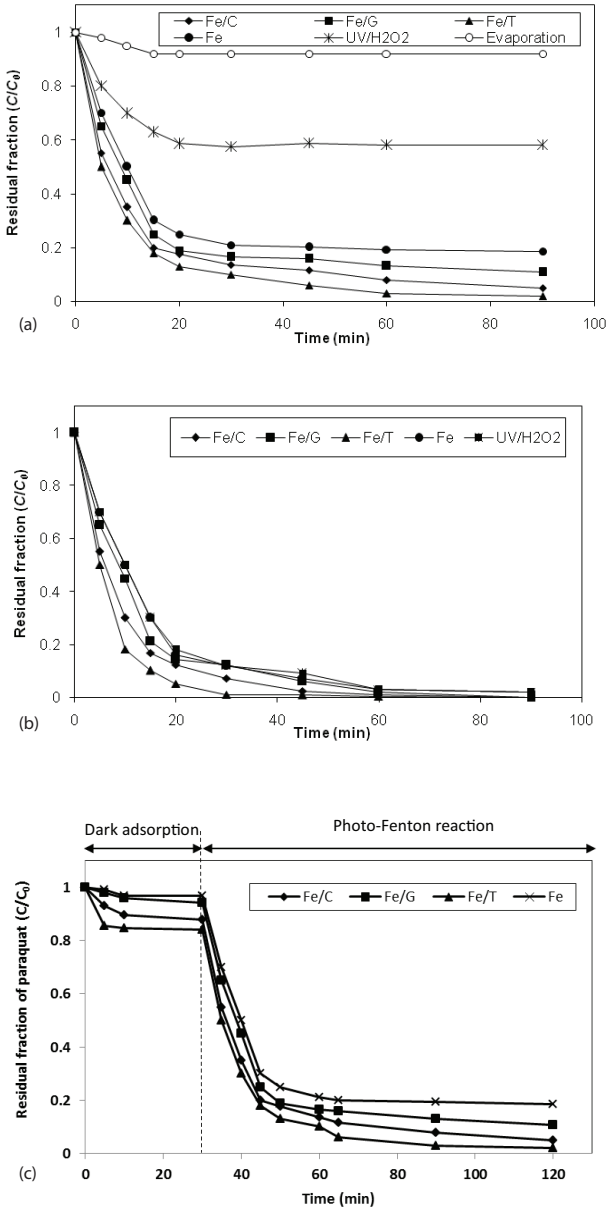

Fig. 8. Comparison of (a) paraquat degradation by photo-Fenton reaction, (b) residual concentration of H_2O_2, and (c) paraquat removal by adsorption and photo-Fenton reaction using various types of green iron nanoparticles in the photo-Fenton process. Conditions: C_0= 200 mg/L, dose of iron nanoparticles = 0.3 g/L, Fe:H_2O_2 = 1:0.8 molar ratio, UV 10 Wt, and pH 3.

Table 4
Values of kinetic parameters including initial rate, *r*, kinetic constant, *k* and half-life of paraquat, $t_{1/2}$, based on the photo-Fenton process of various types of iron nanoparticles

Iron nanoparticles	Kinetic parameters				% Removal efficiency after 50 min	Rate increase
	r (mg/L-min)	$k_{obs} \times 10^{-2}$ (min^{-1})	R^2	$t_{1/2}$ (min)		
Evaporation	0.1200	0.47	0.9449	147.48	8.00	–
UV/H_2O_2	1.0658	2.97	0.9283	23.34	41.83	–
Fe	14.3754	7.27	0.9860	9.53	80.66	–
Fe/G	13.9185	8.56	0.9913	8.10	80.03	1
Fe/C	18.0354	9.82	0.9719	7.06	84.56	1
Fe/T	19.8829	10.94	0.9770	6.34	88.00	2

3.5. Mineralization of paraquat by green iron nanoparticles

The degradation percentage of paraquat regarding mineralization of TOC in the presence of iron nanoparticles in Fenton and photo-Fenton was also investigated. In the Fenton process, the initial concentration of paraquat was 60 mg/L with an initial TOC value of 32 mg/L. In the photo-Fenton process, the initial concentration of paraquat was 200 mg/L with an initial TOC Value of 98 mg/L. The degradation percentage and mineralization to the TOC of paraquat in the Fenton process using four types of iron nanoparticles are shown in Fig. 9 and results for the photo-Fenton process are shown in Fig. 10. In all cases, a rapid degradation of paraquat occurred, and the paraquat concentration decreased after irradiation for 20 min. Mineralization of paraquat for both Fenton and photo-Fenton processes in the presence of Fe from co-precipitation showed the lowest yield. In contrary, among all iron nanoparticles, the Fe/T provided highest TOC percentage removal by both processes.

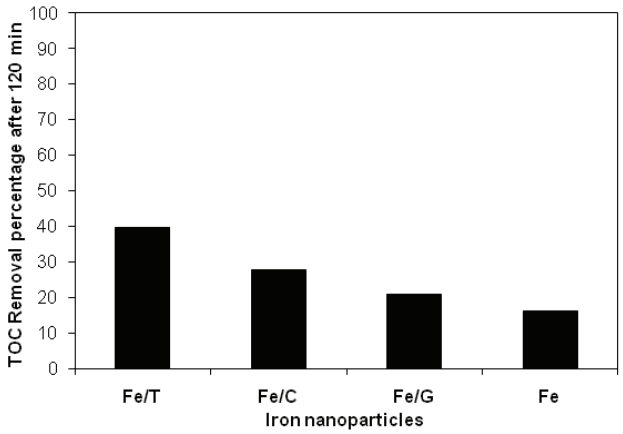

Fig. 9. TOC Removal percentage of paraquat in Fenton process using various iron nanoparticles.

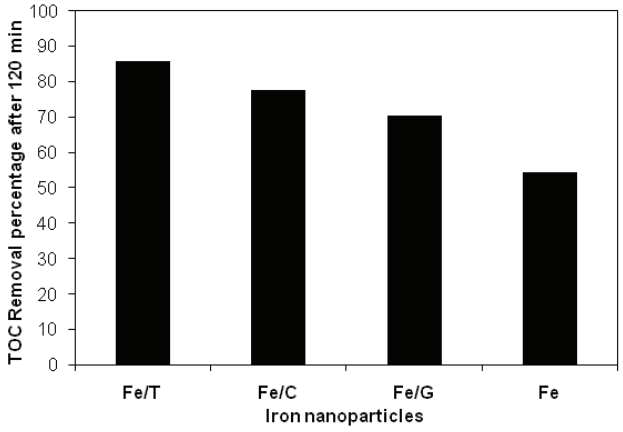

Fig. 10. TOC Removal percentage of paraquat in photo-Fenton process using various iron nanoparticles.

4. Conclusion

Different types of green iron nanoparticles displayed differences in crystal size and pHpzc and consequently, paraquat degradation efficiencies of iron nanoparticles during Fenton and photo-Fenton processes. Results from FTIR spectra of all types of iron nanoparticles exhibited the clear peaks representing the presence of organic molecules from plant extract in the composition of iron nanoparticles. The increasing of crystal size of iron nanoparticles from plant extract illustrated that the organic molecules from extracts tended to cap the iron nanoparticles. These capping agents can prevent the aggregation or agglomeration of iron nanoparticles and enhance the well dispersion of particles in water. Results from zeta potential measurements show that the pH_{pzc} from plant extracts shifted toward a very low pH. The pH_{pzc} of Fe/T, Fe/C, Fe/G and Fe were found at 1.6, 2.2, 3.3, and 4.1, respectively. At pH3, the cationic paraquat was readily adsorbed on a negatively-charged surface of green iron nanoparticles namely Fe/T and Fe/C. The minimal adsorption of paraquat was detected on the surface of Fe/G and Fe. These capping agents of organic chemicals from extracts effectively shifted the pH_{pzc} toward a very low pH. The surface charge of green iron nanoparticles from tea and coffee extracts became negative upon increase of pH beyond the pH_{pzc} and vice-versa.

Amongst four types of iron nanoparticles, Fe/T with lowest pH_{pzc} provided the highest paraquat removal percentage for both Fenton and photo-Fenton processes. Results of the kinetic study show that both processes followed a pseudo-first-order pattern. The initial rate of paraquat degradation of the Fe/T in the Fenton process was 2.63 mg/L-min, and

the kinetic constant was 3.82×10^{-2} min^{-1}. For the photo-Fenton process, the initial rate of paraquat degradation of the Fe/T was 19.88 mg/L-min and the kinetic constant was 10.94×10^{-2} min^{-1}. The paraquat mineralization ability of all iron nanoparticles can be arranged in the following order: Fe/T > Fe/C > Fe/G > Fe.

References

[1] M.B. Brahim, R. Abdelhédi, Y. Samet, Oxidation of the insecticide dimethoate by Fenton and solar photo-Fenton processes using a lab-scale continuous flow reactor, Desal. Wat. Treat., 52 (2014) 6784–6791.

[2] A. Debnath, K. Deb, K.K. Chattopadhyay, B. Saha, Methyl orange adsorption onto simple chemical route synthesized crystalline α-Fe_2O_3 nanoparticles: kinetic, equilibrium isotherm, and neural network modeling, Desal. Wat. Treat., 57 (2016) 13549–13560.

[3] J. He, X. Yang, B. Men, Z. Bi, Y. Pu, D. Wang, Heterogeneous Fenton oxidation of catechol and 4-chlorocatechol catalyzed by nano-Fe_3O_4: role of the interfaces, Chem. Eng. J., 258 (2014) 433–441.

[4] L. Xu, J. Wang, A heterogeneous Fenton-like system with nanoparticulate zero-valent iron for removal of 4-chloro-3-methyl phenol, J. Hazard. Mater., 186 (2011) 256–264.

[5] S.-S. Chen,Y.C. Huang, J.-Y. Lin, M.-H. Lin, Dechlorination of tetrachloroethylene in water using stabilized nanoscale iron and palladized iron particles, Desal. Wat. Treat., 52 (2014) 702–711.

[6] R. Varma, Greener approach to nanomaterials and their sustainable applications, Curr. Opin. Chem. Eng., 1 (2012) 123–128.

[7] X.Q. Li, D.W. Elliott, W.X. Zhang, Zero-valent iron nanoparticles for the abatement of environmental pollutants: materials and engineering aspects, Crit. Rev. Solid State Mater. Sci., 31 (2006) 111–122.

[8] Y. Wang, S. Maksimuk, R. Shen, H. Yang, Synthesis of γ-iron oxide nanoparticles using a freshly-made and recycled ionic liquid, Green Chem., 9 (2007) 1051–1056.

[9] G. Hoag, J. Collins, J. Holcomb, J. Hoag, M. Nadagouda, R. Varma, Degradation of bromothylmol blue by 'greener' nano-scale zero-valent iron synthesized using tea polyphenols, J. Mater. Chem., 19 (2009) 8671–8677.

[10] U.S. EPA., Paraquat Dichloride. Registration Eligibility Decision (RED). U.S. Environmental Protection Agency, Washington, DC, EPA 738-F-96-018, 1997.

[11] J.-C. Lee, M.-S. Kim, B.-W. Kim, Removal of paraquat dissolved in a photoreactor with TiO_2 immobilized on the glass-tubes of UV lamps, Water Res., 36 (2002) 1776–1782.

[12] M.G. Sorolla II, M.L. Dalida, P. Khemthong, Grisdanurak, Photocatalytic degradation of paraquat using nano-sized Cu-TiO_2/SBA-15 under UV and visible light, J. Environ. Sci., 24 (2012) 1125–1132.

[13] M.S.F. Santos, A. Alves, L.M. Madeira, Paraquat removal from water by oxidation with Fenton's reagent, Chem. Eng. J., 175 (2011) 279–290.

[14] F. Mcneil-Watson, W.W. Tscharnuter, J. Miller, A New Instrument for the Measurement of Very Small Electrophoretic Mobilities using Phase Analysis Light Scattering (PALS), Colloids Surf APhysicochemEng Asp, 140 (1998) 53–57.

[15] X. Lu, B.A. Rasco, J.M.F. Jabal, D.E. Aston, M. Lin, M.E. Konkel, Investigating antibacterial effects of garlic (*Allium sativum*) concentrate and garlic-derived organosulfur compounds on *Campylobacter jejuni* by using fourier transform infrared spectroscopy, Raman spectroscopy, and electron microscopy, Appl. Environ. Microbiol., 77 (2011) 5257–5269.

[16] M.C. Mascolo, Y. Pei, T.A. Ring, Room temperature co-precipitation synthesis of magnetite nanoparticles in a large ph window with different bases, Materials, 6 (2013) 5549–5567.

[17] Q. Hua, W. Huang, Chemical etching induced shape change of magnetite microcrystals, J. Mater. Chem., 18 (2008) 4286–4290.

[18] W. Kim, C.-Y. Suh, S.-W. Cho, K.-M. Roh, H. Kwon, K. Song, I.-J. Shon, A new method for the identification and quantification of magnetite–maghemite mixture using conventional X-ray diffraction technique, Talanta, 94 (2012) 348–352.

[19] M.N. Nardagouda, R.S. Varma, Green synthesis of silver and palladium nanoparticles at room temperature using coffee and tea extract, Green Chem., 10 (2008) 859–862.

[20] P. Kajitvichyanukul, M.-C. Lu, A. Jamroensan, Formaldehyde degradation in the presence of methanol by photo-Fenton process, J. Environ. Manage., 86 (2008) 545–553.

Supplementary data

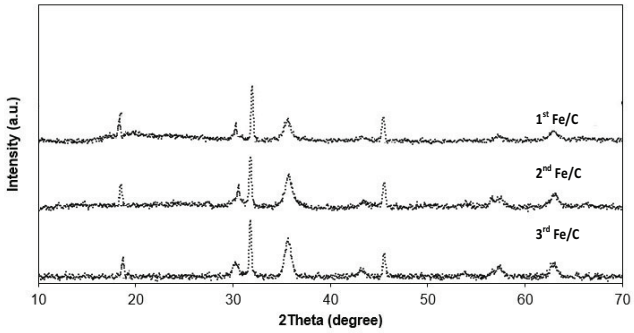

Fig. S.1. XRD spectra of Fe/C from three batches using greensynthesis.

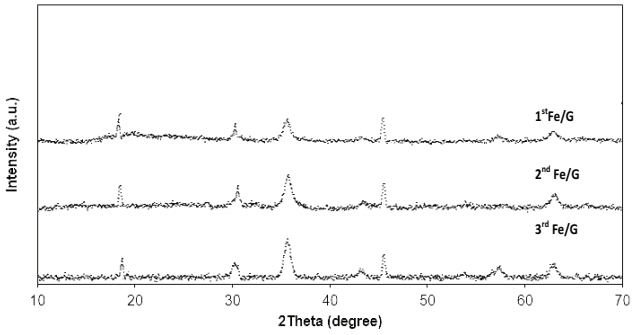

Fig. S.2. XRD spectra of Fe/G from three batches using greensynthesis.

Table S.1
Nanoparticle sizes of Fe/C and Fe/G

Type	Crystal size (nm)		
	1st batch	2nd batch	3rd batch
Fe/G	35.02 ± 11.1	36.78 ± 9.2	36.35 ± 20.8
Fe/C	45.24 ± 14.8	40.02 ± 16.5	42.24 ± 14.9